powders

MDPI

Article

Fast Synthesis of Fine Boron Carbide Powders Using Electromagnetic Induction Synthesis Method

Anna V. Gubarevich * and Katsumi Yoshida

Laboratory for Zero-Carbon Energy, Institute of Innovative Research, Tokyo Institute of Technology, 2-12-1, Ookayama, Meguro-Ku, Tokyo 152-8550, Japan; k-yoshida@zc.iir.titech.ac.jp
* Correspondence: hubarevich.h.aa@m.titech.ac.jp; Tel.: +81-3-5734-2960

Abstract: Boron carbide (B_4C) powders with defined stoichiometry, high crystallinity, minimal impurity content, and a fine particle size are imperative for realizing the exceptional properties of this compound in advanced high-technology applications. Nevertheless, achieving the desired stoichiometry and particle size using traditional synthesis methods, which rely on prolonged high-temperature processes, can be challenging. The primary objective of this study is to synthesize fine B_4C powders characterized by high crystallinity and a sub-micron particle size, employing a fast and energy-efficient method. B_4C powders are synthesized from elemental boron and carbon in a high-frequency induction heating furnace using the electromagnetic induction synthesis (EMIS) method. The rapid heating rate achieved through contactless heating promotes the ignition and propagation of the exothermic chemical reaction between boron and carbon. Additionally, electromagnetic effects accelerate atomic diffusion, allowing the reaction to be completed in an exceptionally short timeframe. The grain size and crystallinity of B_4C can be finely tuned by adjusting various process parameters, including the post-ignition holding temperature and the duration of heating. As a result, fine B_4C powders can be synthesized in under 10 min. Moreover, these synthesized B_4C powders exhibit oxidation onset temperatures higher than 500 °C when exposed to air.

Keywords: boron carbide; powders; electromagnetic induction; synthesis; oxidation resistance

Citation: Gubarevich, A.V.; Yoshida, K. Fast Synthesis of Fine Boron Carbide Powders Using Electromagnetic Induction Synthesis Method. *Powders* **2024**, *3*, 17–27. https://doi.org/10.3390/powders3010002

Academic Editor: Paul F. Luckham

Received: 10 November 2023
Revised: 27 December 2023
Accepted: 3 January 2024
Published: 8 January 2024

1. Introduction

Boron carbide (B_4C) has outstanding properties such as high hardness, low density, high melting point, high temperature stability, good thermoelectric characteristics, and high neutron absorption, making this material attractive for a wide range of applications especially in severe environments, including aerospace, nuclear reactors, and high-temperature thermoelectric conversion [1–3]. B_4C is commonly used in nuclear applications as a neutron absorber [4]. The most recent applications of B_4C include boron neutron capture therapy [5], microwave absorbers [6], and photocatalysts [7]. Boron carbide is known to exist as a single phase with carbon concentrations from 8.8 to 20% [2]. Stoichiometry of boron carbide affects its mechanical, thermoelectric, optical, and other properties [1].

B_4C is commercially produced by the carbo-thermic reduction of boric acid or magnesiothermy in the presence of carbon [3]. High temperatures and long durations, which are necessary in carbo-thermic reduction or magnesiometry, result in a large grain size of the product, requiring time- and energy-consuming steps of crushing and grinding to obtain fine powders, necessary, for example, for fabrication of dense ceramics. Sintering of B_4C is very difficult, therefore the powder size of B_4C must be as low as possible, at least smaller than 3 μm for pressureless sintering (powders with sizes larger than 8 μm cannot be sintered [2]). However, crushing and grinding in air can affect the surface properties of B_4C powders, including their wettability [5]. Pure wettability of B_4C complicates biological applications [5] and fabrication of ceramic composite materials [8].

High-technology applications of B_4C require powders with high purity, precise stoichiometry, and fine particle size [4–7]. Direct synthesis of B_4C from boron and carbon (Equation (1)) can address issues of purity and stoichiometry.

$$4B + C = B_4C, \Delta H = -72.1 \text{ kJ mol}^{-1} \quad (1)$$

Boron and carbon are thoroughly mixed and compacted into pellets, which are then heated at temperatures > 1500 °C [3]. Although this method is more expensive than carbothermic reduction, it is preferable when the boron to carbon ratio and high phase purity are important. Nonetheless, due to long time treatment at high temperatures, the product is coarse and requires crushing, grinding, and ball-milling. Addition of grain growth inhibitors (e.g., tungsten boride) can address the problem of increased grain growth [8]. While recent reports have introduced innovative synthesis methods for B_4C particles with varying sizes and morphologies [6], there is no widely accepted approach for producing high-purity, fine B_4C powders. Moreover, there is an increasing demand to promote environmentally friendly and energy-efficient methods for material synthesis, propelled by efforts to mitigate the climate crisis.

Combustion synthesis, also known as self-propagating high-temperature synthesis (SHS), is a fast, low energy-consuming and low carbon-emission method for the synthesis of ceramic powders including carbides, nitrides, borides, oxides, and more [9,10]. Combustion synthesis exploits highly exothermic chemical reactions, where the heat generated during the reaction promotes and sustains the reaction itself. In a self-propagating mode, the reaction is initiated by a high-energy pulse, such as brief heating achieved by passing an electric current through a tungsten filament. Once ignited, the reaction propagates without the need for additional external energy input. An important parameter for assessing the feasibility of reaction propagation is the adiabatic temperature, which represents the maximum temperature attainable when all the heat generated during the reaction remains within the system. If the adiabatic temperature falls below a certain threshold, typically around 1800 K, the reaction cannot self-propagate. In such cases, alternative techniques like volume combustion (thermal explosion), chemical ovens, or combustion under elevated temperatures may be employed. The direct reaction between boron and carbon is exothermic (Equation (1)), but enthalpy is low (-72.1 kJ mol^{-1}) and the adiabatic temperature is only 955 K, therefore combustion synthesis from elements is not self-sustainable [11]; usually highly exothermic magnesiothermic reaction is used for the combustion synthesis of B_4C in SHS mode [12]. Evidence of an SHS reaction was observed during the field-activated reactive spark plasma sintering of B_4C [11,13]. These findings suggest that, with the appropriate field assistance, combustion synthesis of B_4C is achievable. Recent progress on combustion synthesis of B_4C is presented in [14].

Recently, we introduced a novel synthesis technique, which we refer to as electromagnetic induction synthesis (EMIS), for producing various carbide materials [10,15]. EMIS combines combustion synthesis with the assistance of electromagnetic induction. Electromagnetic induction offers rapid, non-contact, and efficient heating of conductive materials, enabling precise power control and adjustable heating rates over a wide range [16,17]. Therefore, combustion synthesis reactions, even with a limited exothermicity, can be initiated and controlled [10]. Additionally, the electromagnetic field directly impacts the sample, accelerating atomic diffusion and enhancing chemical reactions [18]. By integrating combustion synthesis with electromagnetic induction assistance, it is possible to significantly reduce the time, temperature, and energy required for synthesis when compared to traditional synthesis techniques [10,15].

In this study, we demonstrate the efficient synthesis of fine B_4C powders in a short timeframe using EMIS. The product properties are controlled by optimizing process parameters, including holding temperature and time. Furthermore, we show that the B_4C powders synthesized through this method have high crystallinity which contributes to the improved resistance to oxidation when subjected to heating in air.

2. Materials and Methods

Amorphous boron (0.8 μm, Rare Metallic) and carbon black (80 nm, Asahi Thermal) powders were mixed in stoichiometric proportion with addition of ethanol using a SiC mortar with pestle. Then, powders were dried in vacuum drying oven at 70 °C overnight. After drying mixtures were uniaxially pressed into pellets at 10 MPa pressure. A pellet was placed into a graphite crucible and covered with a graphite lid. The crucible was set in high-frequency induction heating (HF IH) apparatus (MU-αIV, SK Medical Electron, Nagahama, Japan) and heated under high-purity (O_2 < 0.2 ppm) Ar flow. To measure the temperature of the samples, an infrared optical pyrometer (working range 600~3000 °C) was used. Basic experimental set-up is shown in Figure 1a. The optical pyrometer was focused on the graphite lid as shown in Figure 1a. For recording an exothermic peak of the reaction, the graphite lid was taken off and temperature was measured on the top surface of the samples (Figure 1b). The heating program consisted of three steps: preheating at a slow heating rate (300 °C·min^{-1}), ignition at a high heating rate (1000 °C·min^{-1}), and postheating (holding) at constant temperature (1900, 1950, and 1970 °C). Finally, the sample was cooled down naturally under Ar flow. The grey-colored lightly sintered product was obtained. The samples' ID with the details of heating conditions are shown in Table 1.

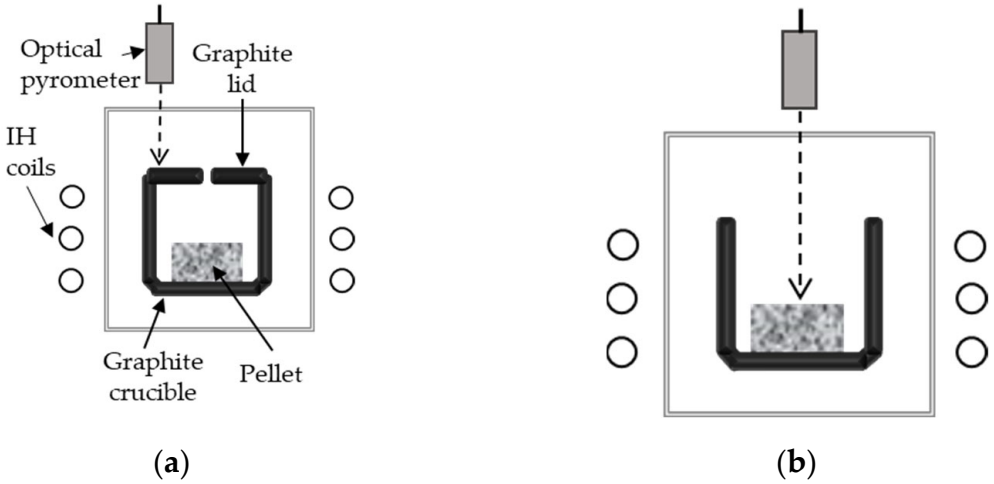

Figure 1. Electromagnetic induction synthesis (EMIS) experimental set-up: (**a**) standard synthesis experiments, (**b**) recording the exothermic peak. Dashed arrows indicate point of temperature measurement.

Table 1. Samples synthesized in the present work.

T_{max} (°C)	Point of T Measurement	Holding Time at T_{max} (min)	Sample ID
1700	Sample	0	1
1900	Graphite lid	3	2
1900		5	3
1950		3	4
1970		0	5

Field-emission scanning electron microscopy (FE-SEM, Hitachi S-4800, Hitachi High-Tech Corporation, Tokyo, Japan) equipped with Energy Dispersive X-ray Spectroscopy (EDX) unit (EDAX, active area 300 mm^2) was applied to characterize microstructure of the fracture surface, grain size and shape of as-synthesized samples, and to measure the oxygen content. In case of the EDX analysis, the samples were fixed on an aluminum holder using a copper adhesive tape; the accelerating voltage was 10 kV and magnification was 2000. The mean grain size and grain size distribution was calculated from the SEM images (more than 600 grains were measured for each examined sample) using ImageJ free software (National Institutes of Health, Bethesda, MD, USA, version 1.54d). The samples were lightly ground

using a silicon carbide mortar and pestle for further analysis. Crystalline phases were determined using X-ray diffraction method (XRD, Aeris, Malvern Panalytical, Eindhoven, The Netherlands). The specific surface area was analyzed by static manometric nitrogen adsorption at cryogenic temperature (77 K) using a Belsorp 28SA apparatus (Microtrack MRB, Osaka, Japan). The samples were outgassed in vacuum at 300 °C for 2 h directly prior to measurement. Calculation of the specific surface area (SSA, A_{BET}) was done according to the Brunauer–Emmett–Teller (BET) theory in the range of 0.05~0.3 partial pressure. Average particle size d (nm) was calculated from A_{BET} ($m^2 \cdot g^{-1}$) and density of B_4C (ρ, 2.52 $cm^3 \cdot g^{-1}$) under assumption of spherical particles using Equation (2):

$$d = 6000/A_{BET} \times \rho \quad (2)$$

Non-isothermal oxidation tests were performed using a thermogravimetry differential thermal analyzer (TG-DTA, 2020SA, Bruker, MA, USA)) in ambient air. Synthesized B_4C powders were put into Pt pans and heated in air from room temperature to 700 °C under heating rate of 10 °C·min^{-1}. Commercial B_4C powder (H.C. Stark, Golsar, Germany, Grade HS, 0.8 μm mean particle size) was measured using the same procedure for comparison. An oxidation onset temperature (OOT) was defined as the temperature at which weight of the sample starts to increase.

3. Results and Discussion

3.1. Ignition of the Reaction, Temperature-Time Profiles, and Mass Loss during Synthesis

Figure 2a shows temperature vs. time profile measured during heating without the graphite lid as shown in Figure 1b. It can be seen from Figure 2a that after 60 s of slow heating the temperature of the pellet was about 600 °C. When the temperature achieved 800 °C, the heating rate was changed from 300 to 1000 °C·min^{-1}. Then, after 30 s of fast heating, a sharp rise in temperature was observed, which started from 1303 °C. The sharp rise in temperature represents the exothermic peak that appeared due to the exothermic reaction between boron and carbon leading to formation of B_4C (Equation (1)). The ignition temperature is close to the values observed in reactive spark-plasma sintering of B_4C [13]. Maximum temperature of the exothermic peak was 1477 °C. It should be mentioned that the values of temperature measured without lids are always lower than measured on the graphite lid under the same IH power. Therefore, actual values of the exothermic peak are expected to be higher, when the graphite lid covers the crucible, providing better thermal insulation. Direct visual observation of sample during heating confirmed sudden rise of light emission (flash) associated with a volume combustion reaction between boron and carbon. After sample reached temperature of 1700 °C, IH power was stopped and sample was allowed to cool down under Ar flow. It can be seen from the profile that temperature of the sample surface decreased from 1700 to less than 1000 °C in 2 min. One example of a typical temperature profile measured on the carbon lid is shown in Figure 2a. There is no temperature peak related to the exothermic reaction due to the low exothermic value of the reaction, which was not enough to affect the temperature of the crucible. Figure 2b shows that temperature can be finely controlled during synthesis.

The evolution of white vapor at ~1380 °C was observed in all samples. This vapor is associated with the elimination of oxygen impurities, primarily in the form of boron oxide (B_2O_3). Boiling point of B_2O_3 is 1860 °C, but its sublimation starts at 1100 °C. Mass loss, determined as the difference in pellet weight before and after synthesis, was observed for all samples. Table 2 shows the mass loss, oxygen content quantified using EDX, and B_2O_3 content derived from the oxygen content for the synthesized powders. For purposes of comparison, the oxygen content in the starting amorphous boron powder and in commercial B_4C powder (as-received) is provided. Additionally, the corresponding mass loss upon heating boron powders under similar conditions in the HF-IH furnace is presented. From the data in Table 2, it is evident that the mass loss during synthesis was minimal for sample 1; the oxygen content in sample 1 was the highest among synthesized powders, indicating that not all oxygen impurities were removed. Samples 2 to 5 exhibit comparable

mass loss values ranging from 6.5 to 6.9%, indicating that the synthesis conditions were adequate for achieving a stable oxygen content. The starting amorphous boron powders contained 3.08 w% of oxygen, equivalent to 14 w% of B_2O_3. It is considered that B_2O_3 present in the starting boron powder serves as the primary source of oxygen impurities in the synthesized samples. During synthesis, these oxygen impurities undergo evaporation, resulting in significantly reduced oxygen content in the synthesized powders compared to the amorphous boron (see Table 2).

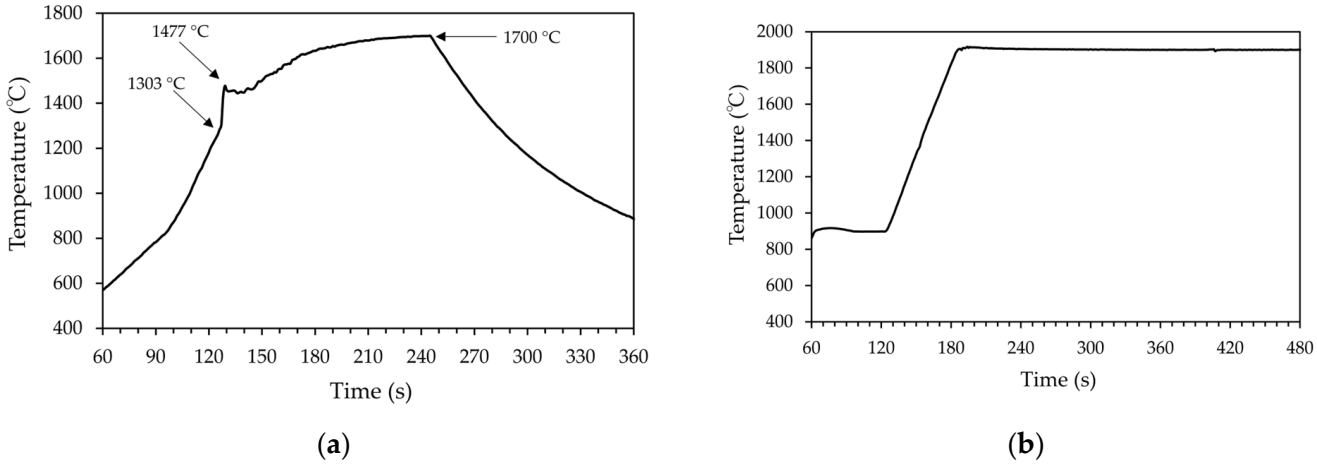

Figure 2. Temperature-time profile during synthesis with temperature measured on: (**a**) the surface of the sample (Sample 1); (**b**) the graphite lid (Sample 3).

Table 2. Oxygen content of synthesized, starting boron and commercial B_4C powders, and mass loss during synthesis (ID 1~5) or heat treatment (Boron).

Sample ID	Oxygen Content		B_2O_3 Content	Mass Loss (w%)
	w%	at%	(w%)	
1	1.18	0.82	5.13	4.2
2	0.64	0.44	2.78	6.9
3	0.89	0.62	3.87	6.8
4	0.84	0.58	3.65	6.9
5	0.58	0.40	2.52	6.5
Boron	3.08	2.10	14.0	9.2 [(1)]
B_4C comm.	0.7	0.48	3.04	-

[(1)] 1900 °C, 5 min heating.

3.2. Characterization of the Synthesized B_4C

3.2.1. Phase Composition

Figure 3 shows XRD patterns of the synthesized B_4C samples. All major peaks were attributed to B_4C. In case of sample 1, peaks of starting materials were observed as well, indicating that the reaction between boron and carbon was not completed at this stage. The exothermicity of the reaction between carbon and boron is not enough to complete the formation of B_4C, therefore some unreacted elemental carbon and boron remained in the sample. Significantly, with the rise in holding temperature from 1900 to 1950 °C, the previously observed broad halos between 22–24 degrees and 35–38 degrees vanished. This suggests an enhancement in phase purity and crystallinity as the temperature increased.

Heating at the rate as fast as 1000 °C·min^{-1} initiates the reaction between carbon and boron due to very high local temperature gradients induced in the sample. Then, the reaction between boron and carbon proceeds via mutual diffusion of carbon and boron atoms. However, the diffusion of boron and carbon atoms in B_4C is a very slow process due to strong covalent bonds between the atoms and high activation barriers.

Moreover, the presence of boron dioxide on the boron particles surface can negatively affect diffusion process. Therefore, in case of sample 1, the reaction between boron and carbon was not completed. When the postheating step at 1900~1970 °C was applied for a short time, the considerable improvement in the phase purity and crystallinity of the samples was observed, indicating acceleration of diffusion under high temperatures. Effective elimination of B_2O_3 (Table 2) could promote diffusion and B_4C phase formation. Additionally, in our previous work [18], it was shown that the induction (eddy) currents induced by high-frequency magnetic field of the coil penetrate through the carbon crucible walls and may affect diffusion processes via electromigration and related phenomena. Therefore, at temperatures beyond 1900 °C, the reaction between boron and carbon was completed in a very short time compared to conventional synthesis [3].

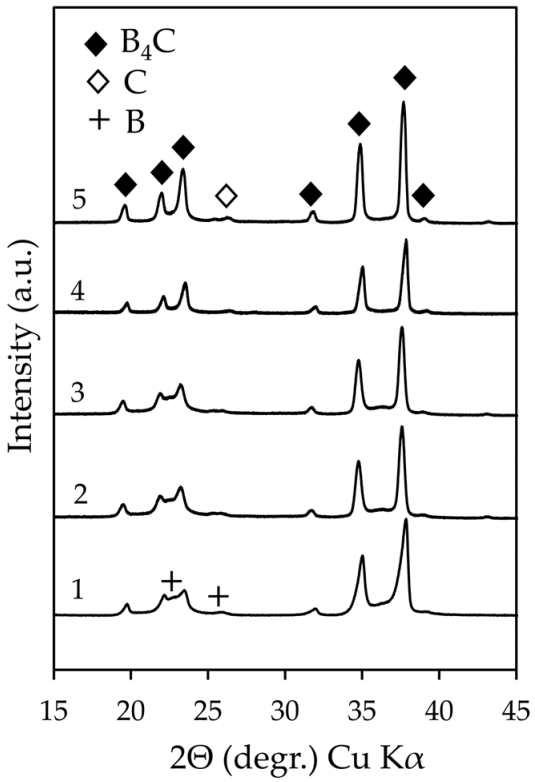

Figure 3. X-ray diffraction (XRD) patterns of synthesized B_4C powders (sample ID numbers are indicated above the respective lines).

3.2.2. Microstructure and Particle Size

Figure 4 shows SEM images of the fracture surface of the synthesized B_4C. It can be confirmed that fine and uniform B_4C grains were synthesized. There was no clear difference in grain shape and size between samples 2 and 3; the grain size is less than 1 μm. Samples 4 and 5 show larger grain size and better-defined grain shape than samples 2 and 3. Across all samples, the grain shape appeared oval with an aspect ratio close to 1. As depicted in Figure 4c,d, heating at 1950 °C and 1970 °C (samples 4 and 5) resulted in the partial sintering of grains, a phenomenon not observed in samples 1 and 2. Previous studies have demonstrated that B_4C particles can self-bond without the aid of low-melting additives films [19], and the assistance of IH promotes sintering of B_4C [18]. Samples 4 and 5 exhibited a step-like relief on the surface of B_4C particles, potentially linked to twinning within the grains [19,20]. The grain size distribution for samples 4 and 5 is shown in Figure 5. It can be seen that sample 5 contains more smaller grains. Although the maximum temperature was higher for the sample 5, no holding time was applied, therefore the heating time in total was much shorter than that of sample 4, leading to a different grain size distribution and smaller grain size. In conclusion, it can be inferred that, when

the maximum temperature during synthesis is 1950 °C and higher, the grain size and morphology develop very rapidly, therefore the optimal temperature is not higher than 1950 °C.

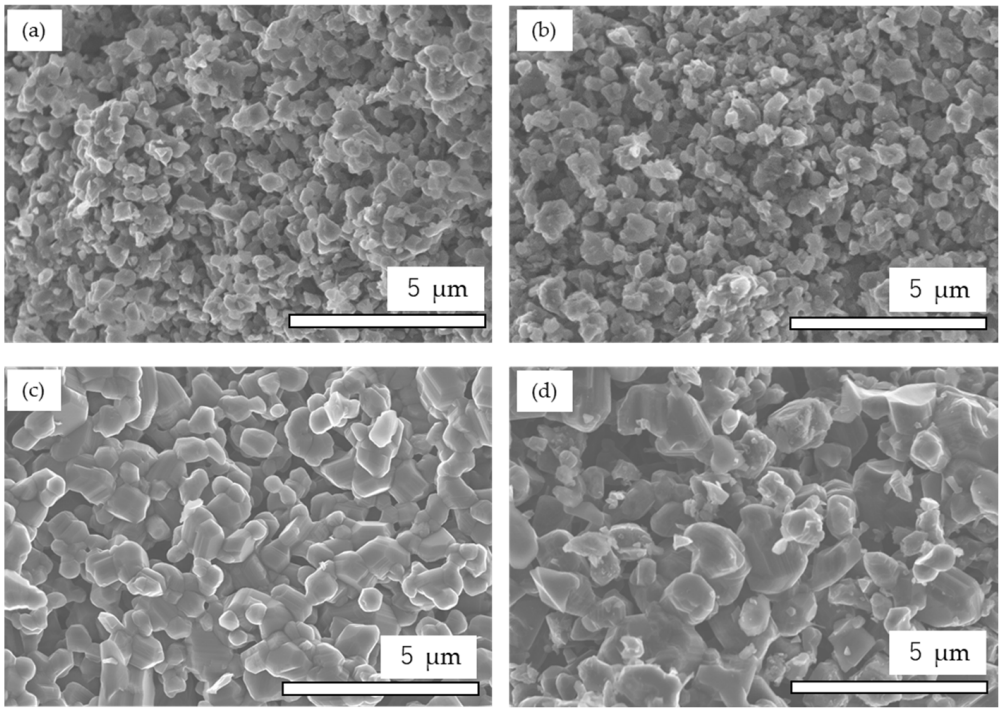

Figure 4. Scanning electron microscopy (SEM) images of synthesized B_4C powders: (**a**) sample 2; (**b**) sample 3; (**c**) sample 4; (**d**) sample 5.

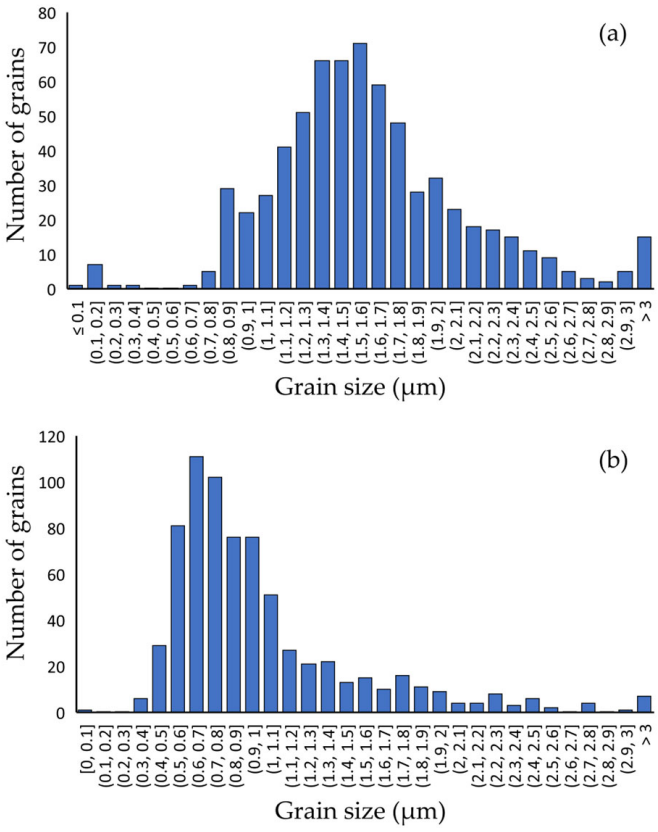

Figure 5. SEM grain size distribution of (**a**) sample 4 (715 grains) and (**b**) sample 5 (678 grains).

3.2.3. Specific Surface Area

Figure 6 shows adsorption and desorption isotherms of the samples 2 and 5. Other samples produced isotherms of similar shapes. The isotherms shown in Figure 6 belong to the type II of the IUPAC classification [21], thus showing that synthesized powders are non-porous or macroporous materials. Hysteresis between adsorption and desorption isotherms can be related to the presence of macropores. Table 3 shows BET specific surface area (SSA, S_{BET}) and average particle size calculated from N_2 gas adsorption data. The SSA of sample 2 is 17.2 $m^2 \cdot g^{-1}$ and an average calculated particle size is 138 nm. The calculated particle size is smaller than that observed by SEM (Figure 4a and Table 3). This discrepancy can be related to the non-spherical irregular shape of the particles. Prolongation of heating at 1900 °C from 3 to 5 min leads to a decrease of the SSA from 17.2 to 11.0 $m^2 \cdot g^{-1}$ and an increase in the average calculated particle size from 138 to 216 nm. As can be seen from Table 3, SEM grain size increased much less. When post-heating temperature was increased to 1950 °C, the SSA decreased to 2.3 $m^2 \cdot g^{-1}$, and average particle size increased to 1035 nm. At this temperature, the SEM grain size was 1600 nm. Heating to 1970 °C leads to a further decrease in the SSA and increase of average particle size. The SEM grain size was smaller than the average particle size. In case of heating at 1970 °C, the sintering of grains is considered to be responsible for discrepancy between the average particle size calculated from N_2 adsorption isotherms and SEM grain size (Table 3).

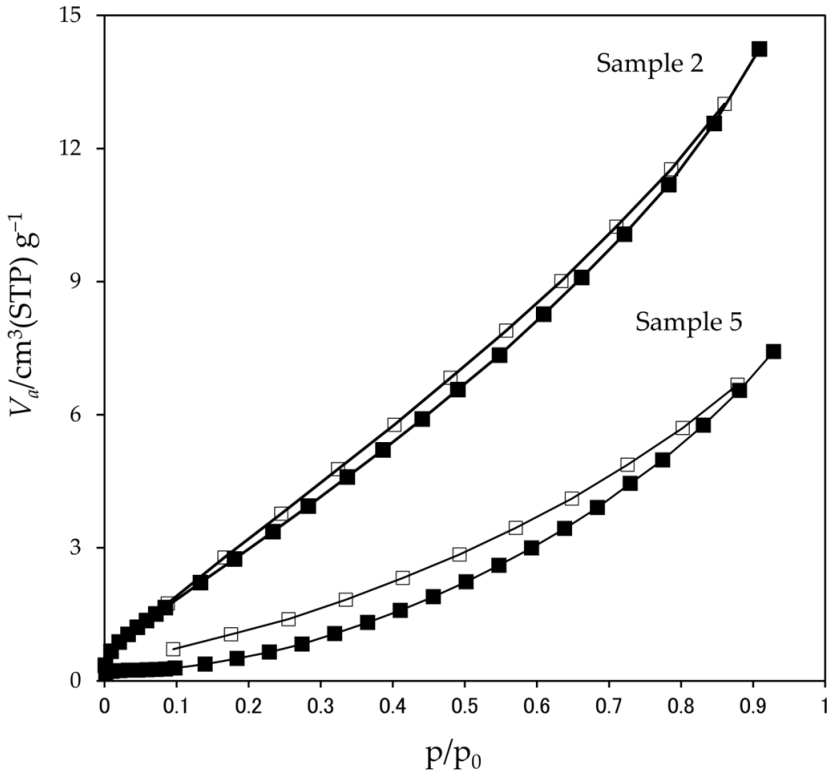

Figure 6. Adsorption (filled squares) and desorption (open squares) isotherms of the samples 2 and 5.

Table 3. Specific surface area, grain size, and oxidation temperature of the B_4C powders.

Sample ID	S_{BET} ($m^2 \cdot g^{-1}$)	Average Particle Size (nm) [1]	SEM Grain Size (nm) [2]	OOT (°C)
2	17.2	138	450	521
3	11.0	216	480	521
4	2.3	1035	1600	584
5	1.5	1550	990	550

[1] Calculated from N_2 gas adsorption. [2] Calculated from SEM images using ImageJ software, version 1.54d.

3.3. Non-Isothermal Oxidation of B_4C Powders

Typical thermogravimetric (TG) curves plotted as weight gain (wt%) versus temperature of the synthesized B_4C powders and commercial B_4C powders are shown in Figure 7. The oxidation of B_4C follows Equation (3) and accompanies a weight gain. The TG curves clearly indicate that there was no measurable weight gain up to 480 °C. The small weight decrease observed in the commercial powder between 200 and 300 °C is related to the decomposition of boric acid formed on the surface of the powders in air. Beyond 480 °C, the weight of the commercial B_4C powder starts to increase rapidly indicating oxidation of B_4C according to Equation (3). The OOT of the commercial B_4C powder, determined as the point on the TG curve where weight starts to increase, was 483 °C. The variation of OOT with the synthesized samples is shown in Table 3. The OOT of all synthesized B_4C powders is higher than that of commercial powder and it increases with increasing post-heating holding temperature from 1900 to 1950 °C. Samples 2 and 3 have very close values of the oxidation temperature, indicating that their stability against onset of oxidation is almost identical. Samples 2 and 3 differ in the postheating time; however, as was shown in Sections 3.2.1 and 3.2.2, their XRD patterns are almost identical, and the grain size measured using SEM differs only by 30 nm. Post-heating at 1950 °C leads to improvement of crystallinity (Figure 3) and increases grain size considerably (Figure 4 and Table 3). As a result, OOT of sample 4 is more than 60 °C higher than that of sample 3. OOT of sample 5, which was heated to 1970 °C, is lower than OOT of sample 4. Sample 5 has a smaller SEM average grain size (Table 3) and its grain size distribution shifted to smaller sizes (Figure 4d), which affects OOT. The particle size has a great influence on oxidation behavior of B_4C powders [22], and our results show strong correlation between SEM grain size and OOT too. The highest OOT was observed for sample 4, which has the largest SEM grain size. Theoretical calculations showed that powders with 1.52 µm particle size have OOT lower than 500 °C [22]. However, OOT of all samples synthesized in the present work exceeds that value. Therefore, it is concluded that OOT is affected not only by the grain size, but by other properties such as crystallinity and stoichiometry of B_4C powders as well.

$$B_4C_{(s)} + 4O_{2(g)} = 2B_2O_{3(s,l)} + CO_{2(g)} \quad (3)$$

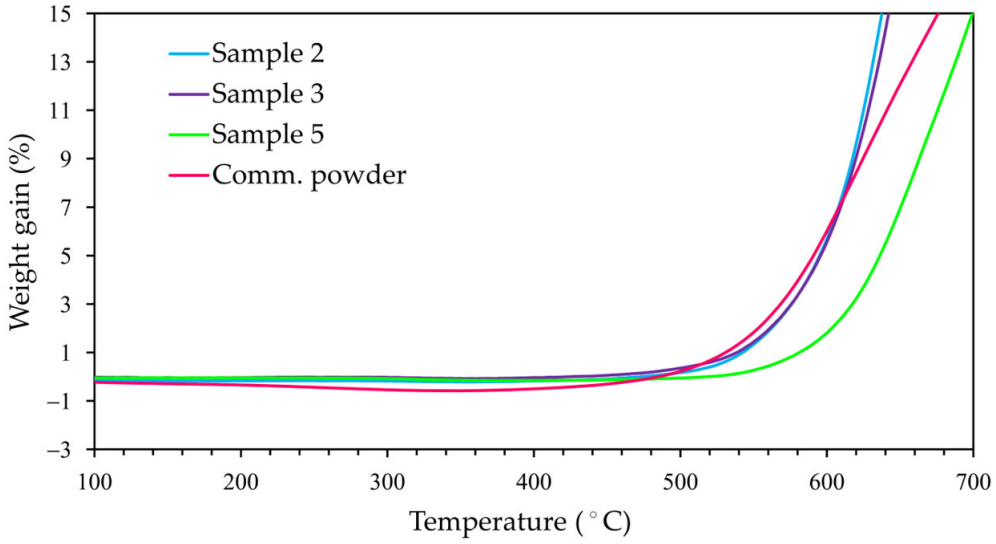

Figure 7. Thermogravimetry (TG) curves of samples 2, 3, 5, and commercial B_4C powder.

As can be seen from Figure 7, beyond 600 °C oxidation proceeds very rapidly. The rate of oxidation of the synthesized powders is higher than that of commercial powder. This behavior can be explained by differences in the thickness of B_2O_3 thin film on the surface of B_4C particles, which forms when the powders are exposed to air during handling. The thickness of the B_2O_3 layer influences the time required for oxygen to diffuse through the

oxide layer, thus affecting the oxidation rate. For an accurate comparison of the oxidation rates between synthesized powders and the commercial powder, standardization of surface conditions is imperative. On the other hand, in contrast to the oxidation rate, OOT was observed to be unaffected by the time elapsed since synthesis and handling conditions. This suggests the possibility that OOT is contingent on the inherent characteristics of B_4C itself, rather than the thickness of the oxide layer.

4. Conclusions

B_4C powders were successfully synthesized through the high-heating rate, high-temperature, and short-time EMIS method. Phase purity and crystallinity were optimized by varying the conditions of a post-heating step. Powders synthesized with post-heating at 1950 °C for 3 min exhibited a graphite-free single-phase composition, a uniform particle size of approximately 1.6 μm, and a high oxidation onset temperature of 584 °C. This surpasses the oxidation onset temperature of commercial B_4C powders by more than 100 °C. In summary, the EMIS method proves to be a promising approach for producing phase-pure, fine B_4C powders, suitable as candidates for advanced technological applications.

Author Contributions: Conceptualization, A.V.G.; methodology, A.V.G.; validation, A.V.G. and K.Y.; investigation, A.V.G.; resources, A.V.G. and K.Y.; data curation, A.V.G.; writing—original draft preparation, A.V.G.; writing—review and editing, A.V.G. and K.Y.; visualization, A.V.G.; supervision, A.V.G. and K.Y.; project administration, A.V.G.; funding acquisition, A.V.G. All authors have read and agreed to the published version of the manuscript.

Funding: This research was supported by JSPS KAKENHI Grant Number 23K04432.

Institutional Review Board Statement: Not applicable.

Informed Consent Statement: Not applicable.

Data Availability Statement: The data presented in this study are available on request from the corresponding author.

Acknowledgments: The authors acknowledge Masamitsu Imai (Tokyo Institute of Technology) for technical support.

Conflicts of Interest: The authors declare no conflicts of interest. The funders had no role in the design of the study; in the collection, analyses, or interpretation of data; in the writing of the manuscript; or in the decision to publish the results.

References

1. Domnich, V.; Reynaud, S.; Haber, R.A.; Chhowalla, M. Boron carbide: Structure, properties, and stability under stress. *J. Am. Ceram. Soc.* **2011**, *94*, 3605–3628. [CrossRef]
2. Thevenot, F. Boron carbide—A comprehensive review. *J. Eur. Ceram. Soc.* **1990**, *6*, 205–225. [CrossRef]
3. Suri, A.K.; Subramanian, C.; Sonber, J.K.; Murthy, T.C. Synthesis and consolidation of boron carbide: A review. *Int. Mat. Rev.* **2010**, *55*, 4–40. [CrossRef]
4. Fajar, M.; Gubarevich, A.; Maki, R.S.S.; Uchikoshi, T.; Suzuki, T.S.; Yano, T.; Yoshida, K. Effect of Al_2O_3 addition on texturing in a rotating strong magnetic field and densification of B_4C. *Ceram. Int.* **2019**, *45*, 18222–18228. [CrossRef]
5. Stodolak-Zych, E.; Gubernat, A.; Ścisłowska-Czarnecka, A.; Chadzińska, M.; Zych, Ł.; Zientara, D.; Nocuń, M.; Jeleń, P.; Bućko, M. The influence of surface chemical composition of particles of boron carbide powders on their biological properties. *Appl. Surf. Sci.* **2022**, *582*, 152380. [CrossRef]
6. Wu, W.W.; Liu, Y.; Zhou, Q.; Liu, L.N.; Chen, X.M.; Liu, P. Microwave absorbing properties of FeB/B_4C nanowire composite. *Ceram. Int.* **2020**, *46*, 4020–4023. [CrossRef]
7. Liu, J.; Wen, S.; Hou, Y.; Zuo, F.; Beran, G.J.; Feng, P. Boron carbides as efficient, metal-free, visible-light-responsive photocatalysts. *Ang. Chem. Int. Ed.* **2013**, *52*, 3241–3245. [CrossRef]
8. Chkhartishvili, L.; Mikeladze, A.; Tsagareishvili, O.; Kvatchadze, V.; Tavkhelidze, V.; Mestvirishvili, Z.; Driaev, D.; Barbakadze, N.; Nadaraia, L.; Sarajishvili, K.; et al. Advanced Boron Carbide Matrix Nanocomposites Obtained from Liquid-Charge: Focused Review. *Condens. Matter* **2023**, *8*, 37. [CrossRef]
9. Patil, K.C.; Aruna, S.T.; Mimani, T. Combustion synthesis: An update. *Curr. Opin. Solid State Mat. Sci.* **2002**, *6*, 507–512. [CrossRef]
10. Gubarevich, A.V.; Watanabe, T.; Nishimura, T.; Yoshida, K. Combustion synthesis of single-phase Al_4SiC_4 powder with assistance of induction heating. *J. Am. Ceram. Soc.* **2020**, *103*, 744–749. [CrossRef]

11. Moskovskikh, D.O.; Paramonov, K.A.; Nepapushev, A.A.; Shkodich, N.F.; Mukasyan, A.S. Bulk boron carbide nanostructured ceramics by reactive spark plasma sintering. *Ceram. Int.* **2017**, *43*, 8190–8194. [CrossRef]
12. Kovalev, I.D.; Ponomarev, V.I.; Konovalikhin, S.V.; Kovalev, D.Y.; Vershinnikov, V.I. SHS of boron carbide: Influence of combustion temperature. *Int. J. SHS* **2015**, *24*, 33–37. [CrossRef]
13. Anselmi-Tamburini, U.; Munir, Z.A.; Kodera, Y.; Imai, T.; Ohyanagi, M. Influence of synthesis temperature on the defect structure of boron carbide: Experimental and modeling studies. *J. Amer. Ceram. Soc.* **2005**, *88*, 1382–1387. [CrossRef]
14. Chkhartishvili, L.; Mikeladze, A.; Chedia, R.; Tsagareishvili, O.; Bugdayci, M.; Karagoz, I.; Maras, T.; Jalabadze, N.; Kvatchadze, V. Combustion Synthesis of Boron Carbide Matrix for Superhard Nanocomposites Production. *Adv. Combust. Synth. Technol.* **2022**, *1*, 66. [CrossRef]
15. Gubarevich, A.V.; Tamura, R.; Yoshida, K. Combustion synthesis of high yield Ti_3SiC_2 from $TiC_{0.67}$ with induction heating assistance. *Ceram. Int.* **2023**, *49*, 23887–23892. [CrossRef]
16. Lucía, O.; Maussion, P.; Dede, E.J.; Burdío, J.M. Induction heating technology and its applications: Past developments, current technology, and future challenges. *IEEE Trans. Industr. Electr.* **2014**, *61*, 2509–2520. [CrossRef]
17. Rudnev, V.; Loveless, D.; Cook, R.L. *Handbook of Induction Heating*, 2nd ed.; CRC Press: Boca Raton, FL, USA; Taylor & Francis Group, LLC.: Philadelphia, PA, USA, 2017.
18. Gubarevich, A.V.; Homma, G.; Yoshida, K. Boron carbide with improved mechanical properties fabricated via rapid pressureless densification with electromagnetic induction assistance. *Scr. Mater.* **2024**, *238*, 115731. [CrossRef]
19. Chen, M.W.; McCauley, J.W.; LaSalvla, J.C.; Hemker, K.J. Microstructural characterization of commercial hot-pressed boron carbide ceramics. *J. Am. Ceram. Soc.* **2005**, *88*, 1935–1942. [CrossRef]
20. Fujita, T.; Guan, P.; Madhav Reddy, K.; Hirata, A.; Guo, J.; Chen, M. Asymmetric twins in rhombohedral boron carbide. *Appl. Phys. Lett.* **2014**, *104*, 021907. [CrossRef]
21. Thommes, M.; Kaneko, K.; Neimark, A.V.; Olivier, J.P.; Rodriguez-Reinoso, F.; Rouquerol, J.; Sing, K.S.W. Physisorption of gases, with special reference to the evaluation of surface area and pore size distribution (IUPAC Technical Report). *Pure Appl. Chem.* **2015**, *87*, 1051–1069. [CrossRef]
22. Hou, X.; Chou, K.C. Quantitative investigation of oxidation behavior of boron carbide powders in air. *J. Alloys Comp.* **2013**, *573*, 182–186. [CrossRef]